Tuijin Jishu/Journal of Propulsion Technology
ISSN: 1001-4055
Vol. 45 No. 4 (2024)

In Vitro Antimicrobial Activity, DFT/ADMET Studies And Molecular Docking of N-Salicylidene-O-Substituted-Aniline as Inhibitors of HERG I and HERG II

Mohamed Yazid Belghit [1]*, Abir Ben Aissa [1, 2], Malika Berredjem [3*], Rania Bahadi[3], Chahra Benzaid[3], Abdelhamid Moussi[4] , Salah Neghmouche Nacer[5] , Ajmal R Bhat[6], Ismahene Grib[3]

[1] *Department Of Process Engineering And Petrochemicals, Faculty Of Technology, University Echahid Hamma Lakhdar, P.O.Box: 789, El-Oued 39000, Algeria.*

[2] *Laboratory of Biotechnology, Biomaterials and Condensed Materials, University of El-Oued, Algeria*

[3] *Laboratory of Applied Organic Chemistry, Synthesis of Biomolecules and Molecular Modelling Group, Sciences Faculty, Chemistry Department, Badji-Mokhtar Annaba University, Box 12, 23000 Annaba, Algeria.*

[4] *Laboratory of Genetic, Biotechnology and Valorization of Bioresources (LGBVB), University of Biskra, P.O.Box 145, RP, Biskra 07000, Algeria.*

[5]*University of El Oued, Faculty of Exact Sciences, Chemistry Department, P.O. Box 789, El Oued 39000,Algeria.*

[6]*Department of Chemistry, RTM Nagpur University, Nagpur, 440033, India*

Abstract

A series of N-salicylidene-o-R-aniline were evaluated against three bacterial strains known to cause human infections: *Staphylococcus aureus (ATCC 25923), Pseudomonas aeruginosa (ATCC 27853), and Escherichia coli (ATCC 25922).* We determined the inhibitory activity of these compounds using two methods: disc diffusion and liquid media dilution. We compared this activity with that of the antibiotic Gentamicin. All compounds confirm a reliable correlation with pharmacokinetic parameters. For specific AMES toxicity, hepatotoxicity, hERG I, and hERG II inhibitors, it is noteworthy that the simulated toxicity model showed greater promise. Particularly the predictive study suggested that these molecular systems have potential therapeutic affinity.

Keywords: N-salicylidene-substituted anilines; HERG.I-HERG.II; antibacterial activity; molecular docking; pharmacokinetic properties; pathogenic species.

1. Introduction

The hazard posed by pathogenic bacteria to human health comes in the form of infectious diseases associated to hospital operations, particularly nosocomial infections. The pathogenic species frequently encountered in these infections are: Escherichia coli, Staphylococcus aureus and Pseudomonas aeruginosa account for approximately 15 to 25% of the germs responsible for these infections [1]. However, to create new antimicrobial drugs, several investigations have been conducted at the platform of research laboratories for the synthesis of chemical structures with their in vitro and in vivo tests on pathogenic microorganisms [2]. In fact, the compounds of the family of Schiff bases [3] which contain the imine function (-CH=N-) have been widely used since the 19th century, due to their extensive biological activity and employment in a different field, including those involving

anti-tumor, anti-microbial, anti-tuberculous, anti-malarial, anti-bacterial, anti-fungal, anti-inflammatory, and antiviral properties [4-8]. As the compound N-(salicylidene)-2-hydroxyaniline inhibits Mycobacterium tuberculosis effectively [9].

In order to orient the synthesis with regard to "drug-like" compounds, it is very important to use the computational approach of virtual screening for the design and evolution of drugs based on the structure of the macromolecule. To prove the potential for biological or therapeutic effect of a compound, it's about the affinity of the interactions of the compound with the protein target. However, by defining the process for estimating the in silico ADME-Toxicity profile (Absorption, Distribution, Metabolism, Excretion and Toxicity), the optimal pharmacokinetic properties of the compound are demonstrated [10-11], this phase makes it possible to create series of compounds having a demonstrated activity on the chosen target. Lack of efficacy in humans and pharmacokinetic issues are two explanations for molecule disappointment during drug development, which can be estimated from its chemical structure, which helps to reduce failures due to these bad properties of ADME-T [12].

In this context, we studied the inhibitory effect in vitro of Schiff's base derivatives (N-salicylidene-o-methylaniline (a), N-salicylidene-o-methoxyaniline (b), N-salicylidene-o-chloroaniline (c), and N-salicylidene-o-nitroaniline (d) are shown in (Figure 1) against the bacteria Staphylococcus aureus, Escherichia coli, and Pseudomonas aeruginosa. Furthermore, we used the virtual screening method for molecular docking of these derivatives with protein targets for a possible design of new bioactive molecules and an evaluation of their ADME-toxicity properties.

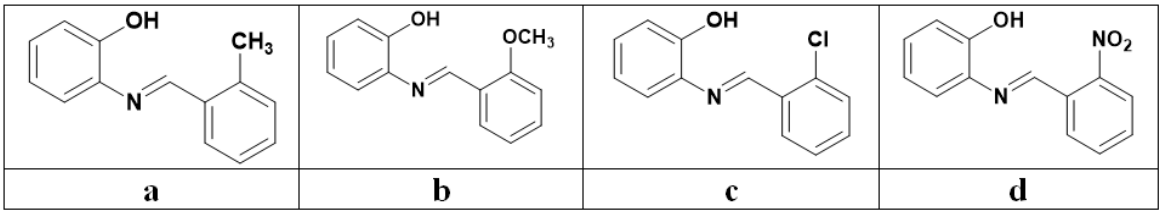

Fig. 1. Structure of the Schiff bases type *N*-salicylidene-O-R-aniline.

2. Results and discussions

2.1. Experimental Study

2.1.1. Variation of the Inhibitory Effect of Schiff's base

The appearance of zones of inhibition reflects the antimicrobial activity of Schiff bases on the bacteria tested.After incubation, the absence of microbial growth is reflected by a translucent halo around the disc, with the diameter of the zone of inhibition (DZI) measured (disc included) and expressed in millimetres (mm). The results are expressed in three levels of activity:

-Résistant: Inhibition zone diameter < 6 mm

- Intermédiaire : 6mm≤ Diameter of zone of inhibition ≤ 13 mm

- Sensible: Diameter of zone of inhibition> 13mm

The results are presented in Table 1.

Table 1. The inhibitory effect of Schiff's base on the bacterial strains studied

Schiff bases	*S. aureus* (+)	*P. aeruginosa*(-)	*E. coli*(-)
	* Diameters of the inhibition zones (mm)		
a	7.83 ± 1.04	9.16 ± 1,04	6.33 ± 0,57
b	8.26 ± 0.76	6 ± 0,00	8.16 ± 0,76
c	7.16±0,76	6.83 ± 0,57	6.33 ± 0,28
d	33±1.00	6.23 ± 1,04	12.16 ± 0,76
DMSO	-	-	-
Gentamicin	27	19	19

*Mean values ± standard deviation (Three tests).

The mean diameters of the various letters vary greatly ($p < 0.05$). The Fisher LSD assay indicates that mean diameters of the same letter are not statistically different at $p > 0.05$. The Schiff bases studied showed different inhibitory activity on the growth of bacterial species. (Figure 2) shows the evaluation of bacterial inhibition in the presence of the Schiff base derivatives tested: In addition, the compound d showed significant activity on the *S.* aureus strain belonging to the Gram-positive bacterial group (33 ± 1, 00 mm) compared with gentamicin with 27 mm of diameter inhibition zone (Figure 3).

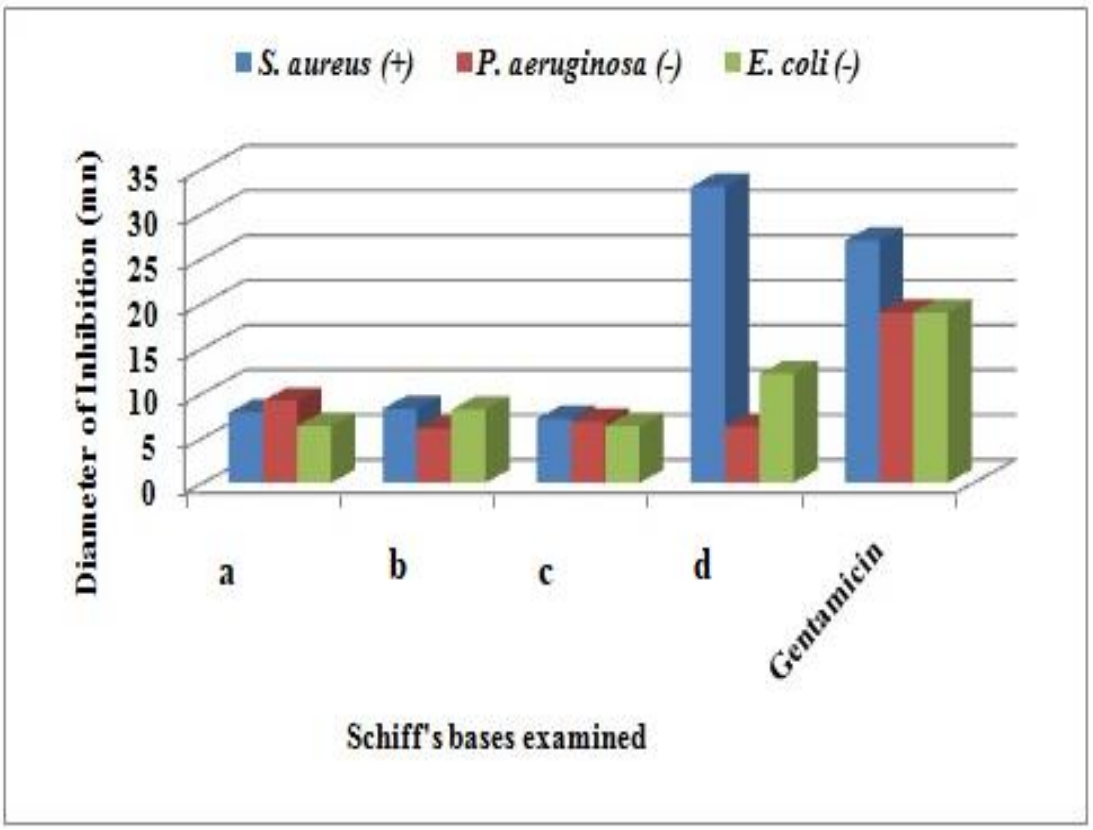

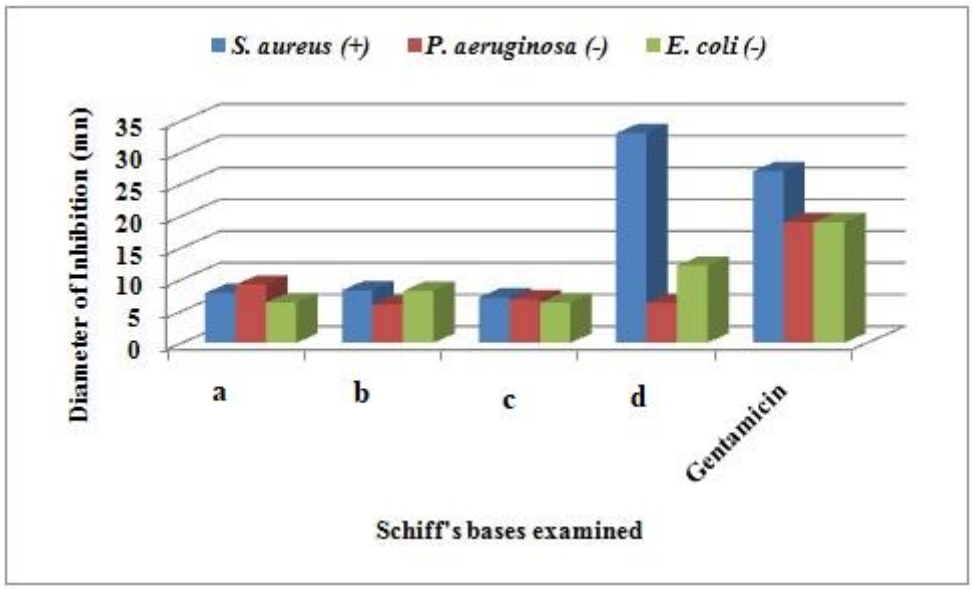

Fig. 2. The variation of the inhibitory activity of Schiff bases against bacterial species

According to the analysis of variance, both the Schiff base and the bacterial species had a significant ($p < 0, 05$) impact on the inhibitory zones. When the inhibition means are compared, the Schiff base d inhibits S. aureus (+) and E. coli (-) strains at $p < 0, 01$ with diameters of inhibition of $33 \pm 1, 00$ and $12, 16 \pm 0, 76$, respectively, when compared to other compounds.

2.1.2. Determination of the MICs and the MBCs

The inhibitory effect of Schiff bases was evaluated by the quantitative identification of MIC and MBC. Indeed, the compounds reveal an inhibition zone with diameters ≥ 9 mm corresponding to the identification of these concentrations. Table 2 summarizes the quantitative activities obtained.

Table 2. The antibacterial properties corresponding to these compounds

Strains	Compounds	MIC	MBC	MBC / MIC	Antibacterial properties,
S.aureus	d	0,25	0,5	2	Bactericidal
P.aeruginosa	a	0,5	>2	ND	Bacteriostatic
E.coli	d	0,5	1	2	Bactericidal

ND: not determined.

2.1.3. Determination of MICs and MBCs

The inhibitory effect of Schiff's bases was assessed by quantitative determination of MICs and MBCs.

The results show that the compound d has very interesting minimum inhibitory and bactericidal concentrations with S. aureus, with concentrations of 0.25 mg/mL and 0.5 mg/mL respectively (Figure 4).

The MBC/MIC ratios indicate the bactericidal (>2) or bacteriostatic (≤2) effect of our molecules.

This compound showed bactericidal activity against S. aureus and E. coli strains. Whereas the compound a showed bacteriostatic power against P. aeruginosa (Figure 5).

The work of [13] reported the antimicrobial activity of Schiff bases in particular: (1) N-(2-Hydroxybenzylidene) pyridine-2-amine, (2) N-(5-nitro-2-hydroxylbenzylidene) pyridine-2-amine, (3) N-(5-bromo-2-hydroxylbenzylidene) pyridine-2-amine, and (4) N-(5-methoxy-2-hydroxylbenzylidene) pyridine-2-amine. demonstrating how different concentrations of these compounds can inhibit the growth of *S.* aureus and *E.* coli.

2.2. Computational Study

2.2.1. Molecular Docking Simulation

Docking begins with importing the protein targets (PDB IDs: 5IQG and 5J5D) and Schiff's base derivatives (in PDB format) into the MVD search space. This procedure comes after a preliminary preparation step that verifies and ensures that the structural properties of each concept are taken into account by the software. We detected five cavities for each protein target, while the cavities designated in our study that contain the ligands co-crystallized with their receptors are located at the level of the main pocket.

These cavities represent volumes and surfaces within the research center, giving it the appearance of a 15Å radius sphere. Table 3 lists the cavities discovered for the two receptors.

Table 3. Property of cavity 1 for each of the protein targets

Proteintargets Code ID : PDB :	Volume ($Å^3$)	Surface($Å^2$)	Position	Bioactive ligands (co-crystallized)
5IQG	1162, 75	2453,76	X=-38, 83; Y= 5, 05; Z= 59,46	51G [a]
5J5D	40,44	145,92	X= 89.38; Y= 97.36; Z= 112.85	6GT[b]

[a]Baicalein: 5, 6, 7-trihydroxy-2-phényl-4H-chromen-4-one.

[b]Bestatin:2-(3-amino-2-hydroxy-4-phenyl-butyrylamino)-4-methyl-pentanoicacid

The receptor-ligand complex formed, adopting the most stable conformation, resulting in the lowest energy level, in the search for the most favorable conformation between the ligand (flexible) and receptor (rigid).

From the perspective of scoring poses, which are produced after 10 research trials by the MVD, the established effectiveness of assessing the affinity and orientation of Schiff's bases in the cavities of active sites allows the classification of the best pose based on the interaction energies obtained at the interaction sites, which are listed in Table 4.

Table 4. MolDock Score interaction energies (kcal/mol) of selected best poses

	5IQG			5J5D		
Ligands	MolDock Score [1]	HBond	Interaction[2]	MolDock Score[1]	HBond	Interaction[2]
a	-81.5727	-2.04268	-91.4015	-78.4573	-5.33511	-89.3033
b	-86.3984	-2.49972	-98.3912	-80.0243	-5.04366	-88.6218
c	-79.0736	-4.99829	-93.0926	-76.9245	-4.64627	-82.5957
d	-89.2204	-6.49797	-103.527	-80.0553	-8.85943	-92.0706
51G	-99.3158	-8.13334	-128.901			
6GT				-82.5957	-8.62594	-93.3023

[1]The sum of external ligand interaction and internal ligand interaction is used to calculate the MolDock score.

[2]The total energy of the protein's interaction with the pose

Most of the poses selected correspond to strong scores and allow you to maintain the best conformation. The complexes formed by the I-4 ligand with the two protein targets have an energy contribution based on the MolDock score of -89, 2204 kcal/mol and -80, 0553 kcal/mol, respectively, which show a significant correlation when compared to the energy contributions made by the 51G and 6GT co-crystallized ligands after docking.

However, modeling of target protein binding sites involved in the conformation of the I-4 inhibitor bound within these crystallographic structures is shown in (Figure 6).

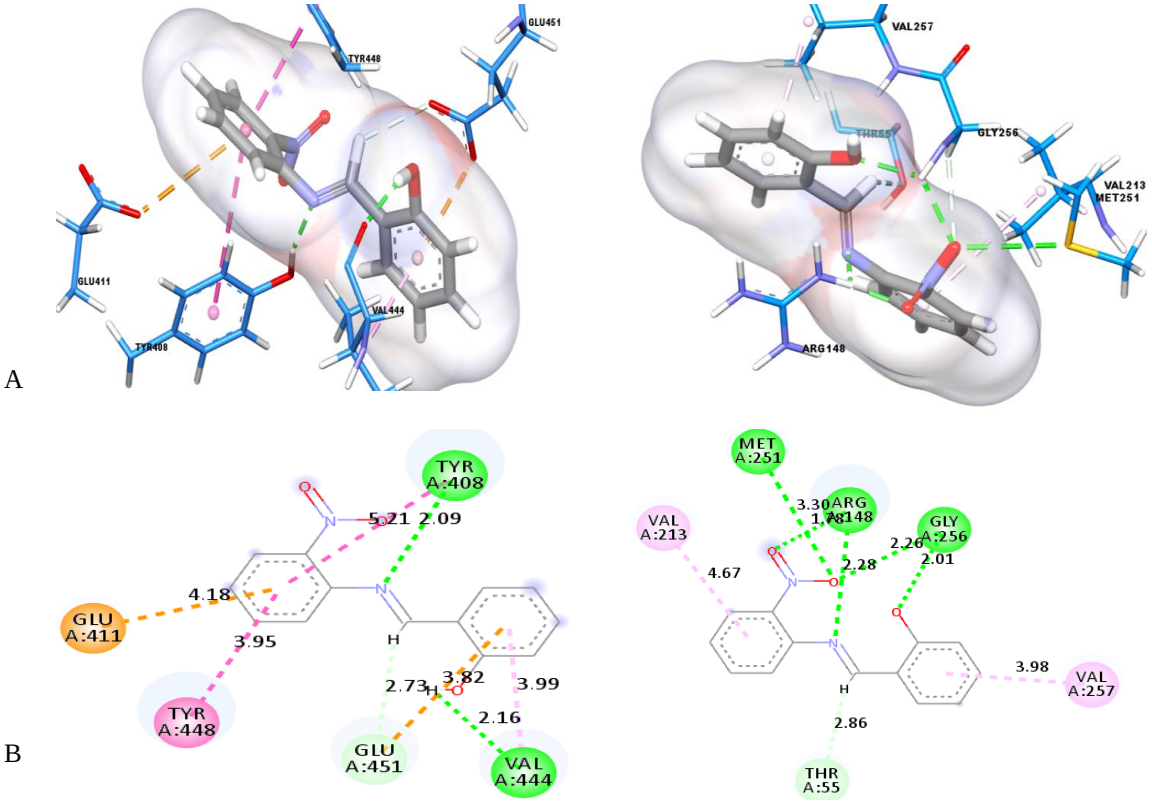

Interaction between I-4 pose and 5IQG Interaction between I-4 pose and 5J5D

Fig.6. Modeling of protein-ligand interactions at the identified binding sites (A) and 2D diagram interactions (B) for each protein target (using the program Discovery Studio 2019)

Each main pocket is identified residues forming the active site through cavity 1. The selection of residues interacting with the I-4 ligand composing the binding site is critical because it guides the calculations and docking results.

The following residues are found in the target protein APH (2″)-Ia binding site: Tyr 408 and Val 444 form hydrogen bonds at distances of 2.09 Å and 2.16 Å, respectively, of which Tyr 448 has established a hydrophobic interaction, while the amino acid Glu411 terminates an electrostatic interaction at a distance of 4.18 Å.In addition, the interaction site of the protein target Mtb-dapA corresponds to hydrophobic interactions by residues Val257 and Val213, while amino acids Met251, Arg148, and Gly256 show hydrogen interactions, although the strongest hydrogen bond revealed is between the amino acid Arg148 and the oxygen atom of the nitro group at a distance of 1.78 Å.

The structural similarity was determined by superimposing these structures and comparing the poses calculated for each ligand with the co-crystal ligand. The arrangement of the calculated conformations is illustrated in (Figures 7a and 7b).

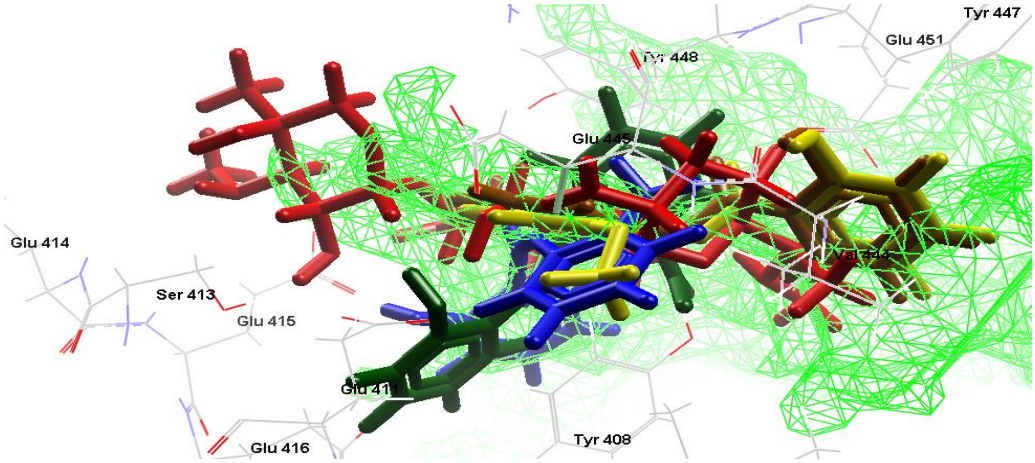

Fig 7a. The superimposition of the conformation of the co-crystallized inhibitor on the predicted optimal position of each ligand within the protein target interaction site APH (2″)-Ia (I-1: blue, I-2: yellow, I-3: brown, I-4: green, and 51GD: re)

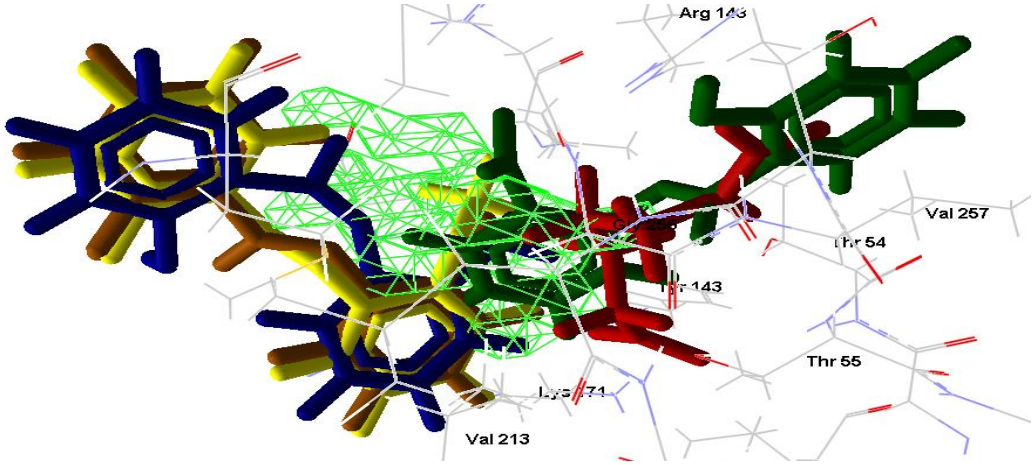

Fig. 7b. The co-crystallized inhibitor conformation is superimposed on the predicted optimal position of each ligand within the protein target interaction site Mtb-dapA (I-1: blue, I-2: yellow, I-3: brown, I-4: green, and 6GT: red).

The formation of a stable complex depends on the interactions between the binding site of the active site of the protein target and the investigated ligands.The modes of interactions corresponding to these complexes formed show a significant similarity in terms of comparison of the nature and the number of bonds with 51G and 6GT; when it comes to the I-4 ligand, its interaction energy is -103, 527 kcal/mol. This energy results from the establishment of two conventional hydrogen bonds, several hydrophobic and electrostatic interactions with the APH receptor (2″)-Ia. Also for the complex formed by Mtb-dapA we obtain five conventional hydrogen bonds and two hydrophobic interactions with I-4 at interaction energy of -92, 0706 kcal/mol. These interaction affinities are significantly higher than those provided by the remains of the ligands (I-2 and I-3).The similarity specificity of the interactions in comparison with the 51G and 6GT ligands is explained as follows:

For 5IQG, two H-donor hydrogen bonds are formed, the first at a distance of 2,09 Å between the hydroxyl group (ID 3 572) of Tyrosine residue (Tyr 408) and the N1 atom of the azomethine group (HC = N... HO), and the second at a distance of 2.73 Å between the oxygen atom (ID 4 264) of glutamic acid (Glu 451) and the hydrogen atom H5 of the azomethine group. Furthermore, hydrophobic interactions of the two phenyl rings of ligand I-4 occurred over distances of 3.94 Å and 3.98 Å, respectively, with the phenyl ring of Tyrosine acid (Tyr 448) and the aliphatic chain of valine (Val 444).

For 5J5D, there are three H-donor hydrogen bonds distributed as follows: The HN group (ID 3 653) of the amino acid Glycine (Gly256) establishes two

hydrogen bonds that are shared with the oxygen atoms (O1 and O3) of the nitro and hydroxyl functional groups over distances of 2.25 Å and 2.01Å respectively. Another H-acceptor hydrogen bond is formed at a distance of 2.85 Å (O... H-C=N) between the oxygen (ID 712) of the amino acid Threonine (Thr55) and the hydrogen of the imine function.

These docking results explain the higher affinity of interaction with protein targets in the presence of I-4 ligand at a large diameter of the inhibition zone, which was 33 ±1.00 for the species Staphylococcus aureus. However, the antibacterial capacity of these compounds was different, according to [14]. This difference is most likely caused by the selective diffusion of the compounds in the bacterial cell membrane.

2.2.2. DFT Study

Molecular Geometry

The optimized geometries of the synthesized N-salicylidene-o-R-aniline (a-d) were studied using the B3LYP 6-31G(d,p) method, employing Gaussian 09 software [15-17].

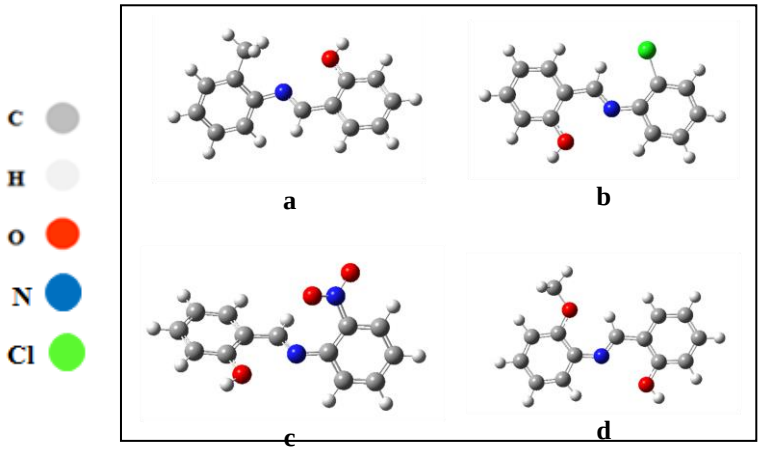

Fig.8. The optimized structure of N-salicylidene-*o*-R-aniline derivatives a-d

Frontier Molecular Orbitals (FMOs)

For biomolecules, computing the frontier orbitals is crucial because they indicate the reactivity centers inside the structure. Throughout the molecule, the highest energy molecular orbitals occupied by electrons are referred to as HOMOs (Highest Occupied Molecular Orbitals [18] (Figure 9).

The gap energy (ΔE) is utilized in order to predict the stability or chemical reactivity of the molecules. all studies molecule has a greater banding gap value (4.204–4.035 eV), but compound C has the lowest value and is thus the most reactive because it is the least stable [19].

Molecules with a higher electrophilicity index tend to engage in a greater number of interactions with biomolecules. Among the four Schiff bases, compound d exhibits a higher electrophilicity index value. molecular docking confirms that compound d was well bound to the 5IQG and 5J5D protein.

Table 5. Calculated EHOMO, ELUMO, ΔEgap, absolute softness (*S*), absolute hardness (*η*), absolute electronegativity (*χ*) and electrophilicity index (*ω*) for all the synthesized compounds 3a-3d at DFT/B3LYP/6-31G(d, p) level.

2.2.2.2. Molecular electrostatic potential

By using an electrostatic potential analysis, the distribution of charges (both positive and negative) within the molecules is found. From the Molecular Electrostatic Potential (MEP), an analysis of the binding and hydrogen bonding interactions between the ligand and the biomolecule may be determined. Different electron charges are represented by the different colors. A negative potential, or attraction to protons, is shown by the color red. Green signifies zero potential, whereas blue indicates a positive potential that indicates repulsion from protons [20-22]. The hydroxyl group was the location of the highest positive zone. This illustrates the likely location of a nucleophilic attack on an oxygen atom with an unshared electron pair. The MEP potential in Schiff bases was found in the

Descripteurs Moléculaire	a	b	c	d
Log P	4.00	4.07	2.80	3.39
μ (D)	2.61	2.14	4.36	4.152
E_{HOMO} (eV)	-5.569	-5.796	-6.132	-5.364
E_{LUMO} (eV)	-1.365	-1.606	-2.097	-1.304
ΔEgap(eV)	4.204	4.190	4.035	4.060
E (u.a)	-671.30	-1091.57	-836.47	-746.50
(η)	2.102	2.095	2.017	1.378
(*S*)	0.476	0.477	0.496	0.726
(μ)	-3.457	-3.701	-2.743	-3.334
(χ)	3.457	3.701	2.743	3.334
(ω)	2.837	3.269	1.865	4.033

hydroxyl group. likewise, the area containing the hydroxyl group and C=N group displayed the greatest amount of hydrogen bonding interactions according to molecular docking. The excellent activity is attributed to the hydroxyl group unit, according to MEP and docking tests. Finding the molecule's electrophilic and nucleophilic sites as well as the MEP, as indicated in (Figure 9), will be made much easier with the use of the molecular electrostatic potential data. incredibly helpful in predicting the chemical system's reaction location

[11].

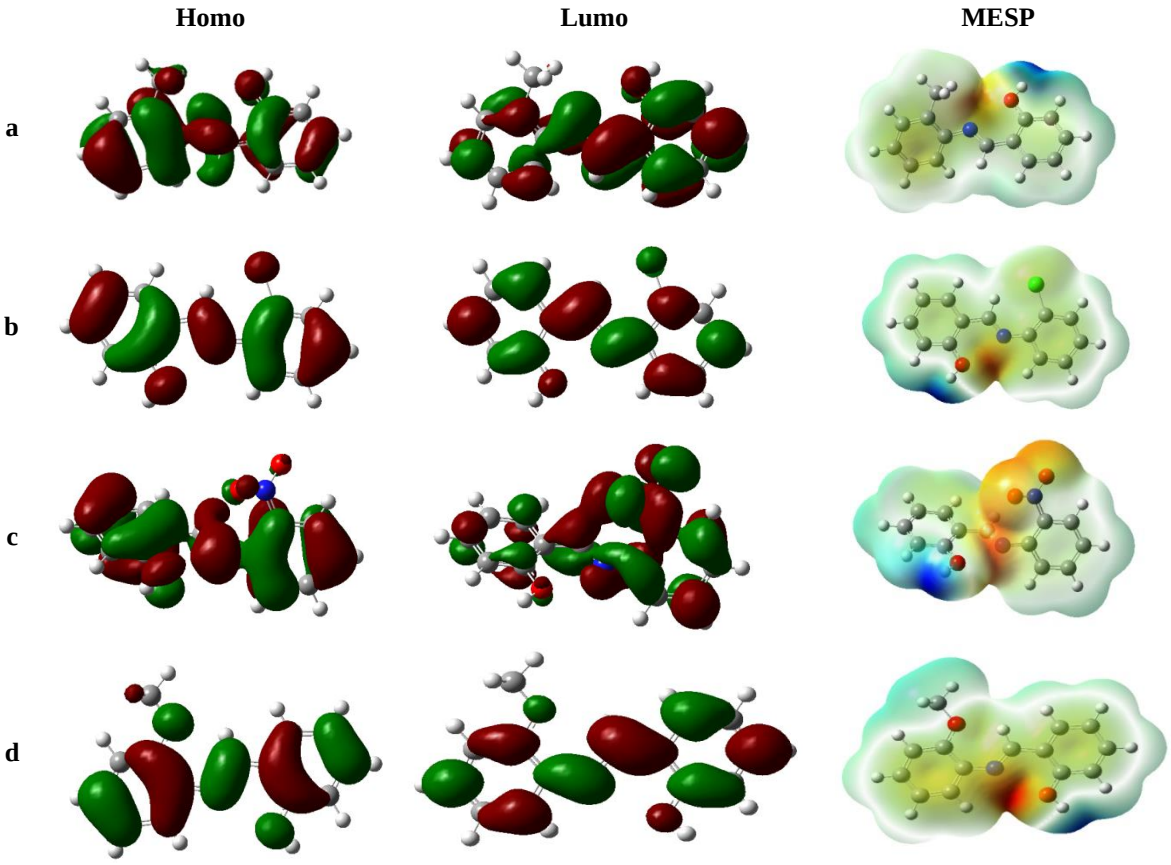

Fig. 9. Frontier orbital and Molecular electrostatic potential maps of compounds a-d

2.2.2. 3. Evaluation of ADME-Toxicity properties

Using the web server (http://biosig.unimelb.edu.au/pkcsm/predicparameters of ADME-toxicity of all ligands were calculated and presented in **Tables 6a, 6b.**

Table 6a. Absorption and distribution properties for these ligands

Properties	Descriptors	Ligands					
		a	b	c	d	51G	6GT
Absorption	Caco2 permeability(log Papp in 10^{-6} cm/s)	1.727	1.723	1.7	0.751	0.979	-0.476
	Intestinal absorption (human)(% Absorbed)	92.845	93.482	91.607	90.668	19.161	34.303
	Skin Permeability(log Kp)	-1.843	-2.63	-2.351	-2.53	-2.735	-2.735
	P-glycoproteinsubstrate	No	Yes	No	Yes	Yes	No
	P-glycoprotein I inhibitor	No	No	No	No	No	No
	P-glycoprotein II inhibitor	No	No	No	No	No	No
Distribution	VDss (human) (log L/kg)	0.364	0.333	0.466	0.284	-1.313	-1.094
	Fraction unbound (human)(Fu)	0.068	0.081	0.083	0.005	0.744	0.669
	BBB permeability(log BB)	0.32	0.11	0.353	-0.273	-0.851	-0.276
	CNS permeability(log PS)	-1.583	-1.7	-1.583	-2.01	-4.093	-3.114

The estimation parameters correspond to the absorption of a compound, such as membrane permeability, which is indicated by the apparent permeability of the Caco-2 cell line, which is used to determine permeability. If a compound has the Caco-2 (Papp) permeability value ≥ 8 $x10^{-6}$ cm / s, it is labeled as having high Caco-2 permeability; otherwise, it is labeled as having moderate-low Caco-2 permeability [23]**.** The percentage of HIA should be greater than 90% and skin permeability (logKp < -2.5) [24,25]**,** while the VDSS, CNS permeability (log PS), and BBB permeability (log BB) are used to predict distribution.

Based on our prediction results, our ligands have better percentages of human intestinal absorption (HIA) with values greater than 90% which are higher than those of the ligands of co-crystallized (51G and 6GT). Additionally, this explains how oral administration of the I-2 ligand with a value of 93.482% could result in greater absorption in the intestinal contour.

The prediction of the membrane permeability factor was moderately permeable through the Caco-2 cell line with log Papp values of 1.727, 1.723, and 1.7 x 10^{-6} cm/s for ligands I-1, I-2, and I-3, respectively, because its apparent permeability values are between 0,9 x 10^{-6} and 10 $x10^{-6}$ cm/s (according to the chemical space classification of the FDA).

It was noted that the estimation of the mucosal transport capacity of these ligands was more acceptable than that of the reference ligands. In addition, when it comes to skin permeability and its “Log Kp” coefficient were less than -2.5, this is true for ligands b (-2.63) and d (-2.53), which exhibit high skin permeability and include both 51G and 6GT ligands (due to log kp < -2.5).However, the decreasing order of the skin permeability capacity of our ligands was as follows: b, d, c, and a.

Furthermore,the predicted ligands can be well distributed in the body. Nevertheless, it is noted that ligands a, b and c showed positive LogBB values (LogBB > 0.3) [19]**.** Consequently, they might naturally traverse the blood-brain barrier, whereas d can moderately penetrate this barrier.On the other hand, the 51G and 6GT ligands shown of the negative values were -0.851 and -0.276, respectively.They will therefore have a poor distribution to the BBB. However, because Log PS >-2 [26]**,** it is easier to predict the entry of ligands a, b, and c into the central nervous system (CNS). While, I-4 ligand showed a value of LogPS = -2.01, suggests moderate penetration of this ligand in the central nervous system. While the 51G and 6GT ligands cannot readily penetrate the CNS, which means the more negative the predicted log PS value is, the molecule will no longer be able to penetrate the CNS.

Notably, the two crucial pharmacokinetic parameters for drug delivery to tissues are unbound fraction (Fu) and volume of distribution (VDss). Despite the fact that drug distribution in tissues is considered high when the VDss value is greater than 0.45, based on the volume of distribution value, [27] described the spectrum of drug distribution. Besides if the value is less than -0.15, this drug has shown poor distribution in the tissues. In point of fact, the ligand I-3 being distributed in the tissues, because it offers the highest predicted value (0.466) compared to the other ligands, it is the VDss value > 0.45. Our ligands can be classified in decreasing order of tissue distribution: I-3, I-1, I-2, and I-4, while the 51G and 6GT ligands may have penetrated more into the plasma than the tissues because they act at VDss values below -0.15 [28]**.**

Table 6b. Metabolism and excretion properties of the studied ligands

Properties	Descriptors	Ligands					
		a	b	c	d	51G	6GT
Metabolism	CYP2D6 substrate	No	No	No	No	No	No
	CYP3A4 substrate	Yes	Yes	Yes	Yes	No	No
	CYP1A2 inhibitior	Yes	Yes	Yes	Yes	No	No
	CYP2C19 inhibitior	Yes	Yes	Yes	Yes	No	No
	CYP2C9 inhibitior	Yes	No	No	Yes	No	No

	CYP2D6 inhibitior	No	No	Yes	No	No	No
	CYP3A4 inhibitior	No	No	No	No	No	No
	Total Clearance	0.154	0.17	0.26	0.393	0.708	0.868
Excretion	(log ml/min/kg)						
	Renal OCT2 substrate	No	No	Yes	No	No	No

Drug metabolism or metabolic alteration of drugs is a xenobiotic biotransformation carried out by oxidation reactions (phase I),which involve the creation or modification of functional groups, and/or by conjugation reactions (phase II) [29]**.** These types of enzymatic reactions take place in the liver to make drugs soluble in more polar water-soluble metabolites more easily eliminated through the urinary or biliary tract.The Cytochromes P450 (CYP) are the main enzymes of phase I, which are composed of different isoforms, including CYP2D6, CYP3A4, CYP1A2, CYP2C19, CYP2C9, CYP2D6, and CYP3A4 involved in drug [30]**.**

It was interesting to observe the predictions about our compounds potential roles as cytochrome P450 monooxygenase system substrates or inhibitors.It was also discovered that these ligands could be well metabolized by CYP1A2 and CYP2C19 inhibitors, whereas I-1 and I-4 become CYP2C9 inhibitors, with the exception of ligand I-3, which becomes a CYP2D6 inhibitor; however, none of them become a CYP2D6 substrate. This is explained by the fact that, due to the complexity of modulation interactions with cytochrome P450 [31]**,** in particular, these ligands were predicted to be substrates of CYP 3A4 and may be metabolites in the liver, suggesting they can be eliminated via the urinary tract without causing significant toxicity [32]**.**

Moreover, the compound's excretion from the body is the most extreme stage of the pharmacokinetic property phases. This is unchanged molecule and / or its metabolites as drugs are excreted through the urinary tract including the liver may participate in the elimination of drugs via the biliary system [33]**.** Total clearance and organic cation transporter 2 substrates were predicted as excretion process parameters.

This shows that a variability of total clearance values was obtained, namely that I-4 ligand showed the highest value, suggesting that this ligand is excreted relatively faster than other derivatives. With the exception of the 51G and 6GT ligands show the highest values of total clearance. We suggest that the excretion of all of Schiff's base derivatives can be considered by the kidneys with a mechanism other than OCT2 [34,35], except for the I-3 derivative, which is a renal absorption transporter, which could be the substrate of the organic cation transporter (OCT2).

2.2.2.3. Lipinski Rules

We proceeded to filter the compounds having the most similar physicochemical properties with the ligands known to be active on the protein target, also the molecules having characters capable of making them drugs otherwise called "drug-likeness". Typically, a molecule is considered drug-like if it meets at least 3 criteria of Lipinski's 5 rules (lipophilicity, molecular weight, molar refractivity, hydrogen bonding, and rotatable bonds) [36].

Additionally, [37] added two more criteria. It is required to find the PSA, which must be < 140 Å², and the number of rotational bonds, which must be less than 10 for the compound.This rule states that when a drug exhibits more than one violation, it is more likely to have low oral bioavailability.

In order to apply this rule to refine a prediction, a study was carried out in particular on the physicochemical properties, medicinal chemistry data, and druglikeness of each ligand, as obtained by swissADME online software (Tables 7a and 7b).

Table 7a . The results of the physicochemical property, lipophilicity, and water solubility criteria

Physicochemical Properties	Lipophilicity	Water Solubility

Ligands	MW (g/mol)	F Csp3	Rb	H-acc	H-don	M-ref	TPSA Å²	Consensus Log $P_{o/w}$	Log *S* (ESOL)	Class
I-1	211.26	0.07	2	2	1	67.13	32.59	3.20	-3.75	Soluble
I-2	227.26	0.07	3	3	1	68.65	41.82	2.84	-3.50	Soluble
I-3	231.68	0.00	2	2	1	67.17	32.59	3.41	-4.04	Moderately soluble
I-4	242.23	0.00	3	4	1	70.98	78.41	2.02	-3.48	Soluble
51G	477.60	1.00	7	12	8	118.31	199.73	-2.15	0.24	Highly soluble
6GT	174.15	0.57	6	5	2	39.51	91.67	0.06	-0.41	Very soluble

The calculation results show that our ligands agree with the Lipinski rules, moreover perfectly within the range of the criteria imposed by the Veber rule. This suggests that these ligands are theoretically capable of exhibiting biological activities and would not have problems with oral bioavailability, overall, to promote intestinal absorption and brain penetration, particularly in terms of physicochemical properties [38].

Table 7b. **The values of the criteria of Drug likeness and Medicinal Chemistry**

	Drug likeness						Medicinal Chemistry			
Ligands	Lipinski violation	Ghose	Veber	Egan	Muegge	Bioavailability Score (F)	PAINS alert	Brenk alert	Leadlikeness violations	Synthetic accessibility
a	Yes; 0	Yes	Yes	Yes	Yes	0,55	0	1	No;1	2.32
b	Yes; 0	Yes	Yes	Yes	Yes	0,55	0	1	No;1	2.42
c	Yes; 0	Yes	Yes	Yes	Yes	0,55	0	1	No; 2	2.32
d	Yes; 0	Yes	Yes	Yes	Yes	0,55	0	3	No;1	2.73
51G	No; 2	No; 2	No; 1	No;1	No; 4	0,17	0	0	No;1	6.51
6GT	Yes; 0	No;1	Yes	Yes	No;1	0,56	0	1	No;1	1.47

It's possible that all ligands effortlessly traverse the BBB and the gut because there are less than five hydrogen bond donors and less than ten hydrogen bond acceptors. This is explained that the more these ligands are able to form hydrogen bonds, the less they would be exerted to diffuse passively into the membranes and therefore to enter the brain [39].

Thus, they can easily pass through the cell membrane according to the molecular weight of all our ligands, with values between 211, 26 and 242, 23 g / mol (less than 500 g / mol).

In particular, this weight margin has suggested that brain penetration of these ligands will be easy [40]. Surprisingly, the larger the volume of the molecule, the more easily it will cross the BBB [41]. Noting that our ligands can be absorbed through the intestine according to the predicted PSA values. Except for the 51G ligand presented a value greater than 140Å2 was 199, 73 Å2. It appears that the PSA is negatively correlated with the logBB and the Caco-2 permeability [42].

However, passive diffusion transport through a cell membrane is proportional to the molecule's partition coefficient.This is positive for our ligands; therefore, 0 < Consensus Log Po/w< 5 to cross the gut, or logP, is

positively correlated with logBB.Indeed, our ligands reveal a very sufficient lipophilicity, which will diffuse more easily through the membranes and penetrate more easily at the cerebral level [43]. Concerning molecular flexibility, [44] have shown that moderate molecular flexibility increases logBB but if the too flexible molecule will not cross the BBB. This explains why our ligands easily penetrate the BBB; it appears that [45] proposed the idea of intestinal absorption increasing with the number of rings and rigid bonds.

Otherwise, we observed that I-1, I-2, and I-4 ligands correspond to classes soluble in water, while I-3 ligand belongs to the class moderately soluble in water showed a lowest value of Log Swas -4.04, accordingly the probability of diffusion of this ligand to cross the barrier made up of cell membranes will be the easiest. However, [46] have demonstrated that the polarity factor has a greater influence on the cerebral passage than does lipophilicity. We can also appreciate through the rate of molar refractivity (between 40 and 130), that these ligands enter the intestine [47].

On top of that, our ligands absorbed at the intestinal level exhibit physicochemical and structural properties that are consistent with data in the literature for drug [48]. They obey Lipinski's rule of five; the same is true for BBB permeability, for which polarity is an important factor of passage, which has also been described for drugs. When analyzing the differences between the values of these descriptors obtained, including their filtering, we observed that a ligand active by the oral route must meet the criteria outlined above.It emerges from these calculations that no violation of Lipinski parameters was predicted for our ligands, which showed the same bioavailability score (F) of 0.55 with good drug likeness according to the rules of Veber, Egan, and Muegge.

Nevertheless, the PAINS and Brenk properties were used to determine different molecular fragments of ligands, which tend to react with different biological targets. Furthermore, these ligands did not reveal any predicted violation of this PAINS property.

Cerebral penetration and intestinal absorption were evaluated by an in silico BOILED-EGG model based on polar and lipophilicity factors [49] Figure 8 shows this model.

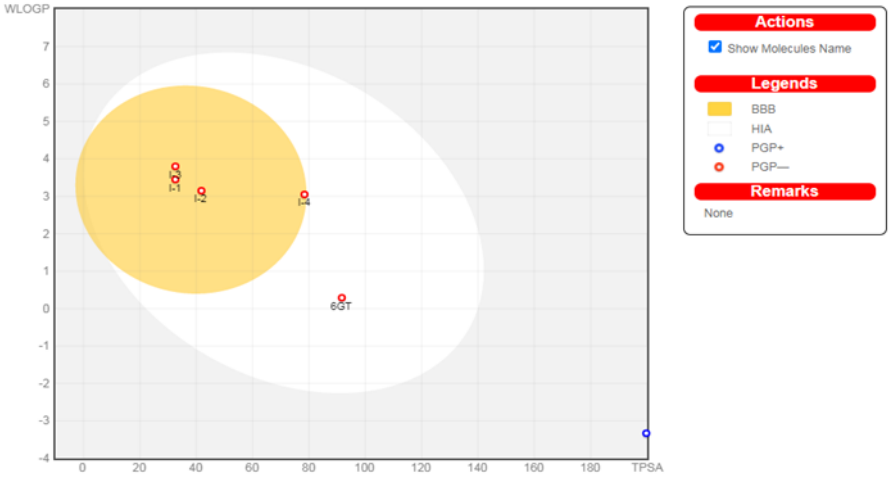

Fig. 10. BOILED-Egg / SwissADME model corresponding to these ligands

A significant proportion of the ligands (66.66%) located inside the yellow ellipse are predicted to diffuse at the BBB, corresponding to the derivatives of the Schiff bases that define good cerebral permeability; these derivatives are also associated with an expected high gastro-intestinal absorption [50].

The 51G and 6GT ligands, which failed for blood-brain barrier permeability with their agglomerations outside the yellow ellipse, except that the prediction of gastro-intestinal absorption was poor for 51G, which was believed to be non-permeable to the brain, displayed the highest tPSA value (tPSA = 199.73Å2) and therefore cannot easily cross cell membranes because it has a low liposolubility with WLOGP = -3.33.

2.2.2.4. Toxicity

In terms of toxicity prediction, which is the most important aspect of drug development failure [51], we used the Pkcsm-pharmacokinetics web server to assess the toxicity of ligands based on significant descriptors: LD50, AMES toxicity, hypatotoxicity, and skin sensitization. The results of the predicted descriptors are grouped in Table 7c.

It appears from this prediction result that the ligands I-2, I-4, 51G and 6GT showed no mutagenic power based on the AMES test, as well as did not cause skin sensitivity. In addition, all the ligands studied do not show an effect on the hERG I and II genes, the inhibition of which could cause cardiac fibrillation and have neither neurotoxic nor hepatotoxic effects. It should be emphasized that the potential mutagenic effect and the skin sensitization effect of ligands I-1 and I-3 can be corrected during the optimization of these ligands.

Table 7c . Significant descriptors of toxicity for all ligands

Descriptors	Ligands					
	a	b	c	d	51G	6GT
AMES toxicity	Yes	No	Yes	No	No	No
Max. tolerated dose (human)(log mg/kg/day)	0.67	0.48	0.646	0.334	0.188	0.73
hERG I inhibitor	No	No	No	No	No	No
hERG II inhibitor	No	No	No	No	No	No
Oral Rat Acute Toxicity (LD50)(mol/kg)	2.012	2.163	2.274	2.434	2.559	1.762
Oral Rat Chronic Toxicity (LOAEL)(log mg/kg_bw/day)	1.111	1.462	1.059	1.292	2.763	2.598
Hepatotoxicity	No	No	No	No	No	No
Skin Sensitisation	Yes	No	Yes	No	No	No
T.Pyriformis toxicity(log ug/L)	1.92	1.388	1.687	1.734	0.285	0.226
Minnowtoxicity(log mM)	0.672	0.385	0.454	0.098	6.242	2.129

3. Materials and methods

3.1. Chemistry Material

The Schiff bases to be tested (Figure 1) were prepared in the laboratory of molecular chemistry and environment at Mohamed Khider University, Biskra, Algeria [52].

The bacterial strains used in this study were reference strains supplied by the bacteriology laboratory of the Hakim Saadan Hospital, Biskra, Algeria. The three reference strains were Staphylococcus aureus (ATCC25923) (Gram +), Pseudomonas aeruginosa (ATCC27853) (Gram -) and Escherichia coli (ATCC25922) (Gram -).

Antibacterial tests (in vitro) Diffusion method on Mueller-Hinton agar medium:

The bacterial suspension was prepared in a saline solution (1 ml of physiological saline solution) and homogenised to a density equivalent to the turbidity standard of 0.5 McFarland using a densitometer. The culture medium (Mueller-Hinton agar) was then inoculated with a sterile cotton swab containing 106 colony-forming units/ml of bacterial suspension. The test solution (5 µL at a concentration of 40 mg/mL in DMSO) was impregnated onto sterile 6 mm diameter Whatman No. 01 paper discs, which were then placed on the inoculated agar; 3-4 discs per Petri plate.

In parallel, discs impregnated with the antibiotic gentamicin and DMSO were used as positive and negative controls, respectively. After incubating the Petri dishes at 37°C for 24 hours, the diameter of the zone of inhibition was determined in millimetres.

Liquid dilution method:

Minimum inhibitory concentrations (MICs) and minimum bactericidal concentrations (MBCs) were determined by the dilution method [53]. A stock solution was prepared by mixing a 100 µL volume of Schiff stock solution with 1800 µL of Mueller-Hinton liquid, giving a total volume of 1900 µL at a C0 concentration of 2.1 mg/mL.

Then, by preparing successive dilutions of the stock solution (C0), namely C01/2, C0 1/4, C0 1/ 8, C0 1/ 16, C0 1/ 32 and C0 1/ 64 up to a volume equal to 950 µL for each tube. Next, 50 µL of bacteria were added to each (inoculum) tube. Incubation was performed at 37°C for 18 to 24 hours to visually detect bacterial growth by the presence of cloudiness: This concentration responds to the lowest concentration of solution inhibiting bacterial growth in these tubes.

The BMC was obtained by inoculating the contents of the tubes (which show the MIC) into Mueller-Hinton agar and determining the BMC, which results in the absence of bacterial growth after 24 hours of incubation at 37°C

Three tests for each sample were used in the antibacterial activity assays, and the results were expressed as mean and standard deviation. Analysis of variance by factor (ANOVA) was used to assess significant differences ($p < 0.05$), and Fischer's least significant difference (LSD) test was used to compare means. STATISTICA software, version 8.0, was used to perform this analysis (StatSoft Inc., Oklahoma USA).

3.2. Molecular Docking Simulations

In the present work, we became interested in predicting the affinity of compounds towardthree-dimensional crystal structures of target proteins APH (2″)-Ia from isolates Staphylococcus aureus (ID: 5IQG)and Dihydrodipicolinate Synthase rom Mycobacterium tuberculosis / Mtb-dapA (ID: 5J5D) [54].

These structures were primarily obtained through X-ray diffraction and were accurately defined with good resolutions (2.50 and 2.40 Å). In order to make the proteins suitable for a study of our ligands docking favorably at their sites of interaction, cofactors, co-crystallized ligands, and water molecules have been removed from the proteins. Version 5.5 of Molegro Virtual Docker (MVD), created by Molegro ApS (2012), was used for the molecular docking technique of Schiff bases.

However, the algorithm embedded in the software allowed us to detect cavities present in protein targets, as well as based on the implications of the MolDock Score, which enhanced the PLP (piecewise linear potential) score functions.

The default settings included the maximum iterations of 1500, the maximum population size of 50, and the energy threshold of 100. These settings were used in conjunction with the MolDock Score function with a grid resolution of 0.30 and a radius of 15, and the MolDock SE search algorithm with a number of runs of 10. Additionally, the neighbor distance factor for the simplex evolution was 1.00, with a maximum step size of 300.

3.3. In silico ADME-Toxicity properties

To learn more about estimating and improving these pharmacokinetic and toxicological properties using a "pKCSM" prediction platform that is freely available from the website (http://structure.bioc.cam.ac.uk/pkcsm) [55], it was crucial that we finish our study by predicting the ADME-toxicity properties of compounds, namely; its absorption, distribution, metabolism, excretion, and toxicity. Additionally, predictions of Lipinski's rule of five, its expansions, pharmacological similarity, and physicochemical parameters describing substances have been made via the swiss ADME web server (http://www.swissadme.ch) [56]. The "Lipinski" rule of five provides an estimate of a compound's oral bioavailability in the body based on its 2D structure.

4. Conclusions

In this study, the inhibitory effect of Schiff base derivatives on human pathogenic bacterial species was examined by the disc diffusion method as a function of substituted groups on the aniline ring at the ortho position.We observed that the presence of several groups, including methyl, methoxy, chloro, and nitro, can be used to explain the diversity of abilities to limit the growth of these bacteria.In order to evaluate and develop our experimental assays in vitro, we verified the effectiveness of the in silico approach.The results of the calculations show that our ligands are in agreement with Lipinski's rules, moreover perfectly within the range of the criteria imposed by the rule of Veber. This suggests that these ligands are theoretically capable of exhibiting biological activities, especially in terms of physico-chemical properties, would not have oral bioavailability problems, promote intestinal absorption, and have cerebral penetration. We used molecular docking simulations and ADME-toxicity criteria to predict the likelihood of inhibition of protein targets APH (2″)-Ia from Staphylococcus aureus isolates and Dihydrodipicolinate Synthase from Mycobacterium tuberculosis (Mtb-dapA). In terms of prospects, our ligands from this work can be used as lead compounds, with interesting optimization to design drugs for specific infectious diseases.

Acknowledgement

The authors gratefully acknowledge the thanks of the Directorate-General of Scientific Research and Technological Development (DGRSDT). We also thank the head, "Dr. Khalad Khelil," of the bacteriology laboratory at Hakim Saadane Hospital, Biskra, Algeria

References

[1]. *M.Guibert, C. Boithias,*Neonatal nosocomial infections. Ther. Med. Pediatrics, 2, 1999, 103.

[2]. *J. Davies, D. Davies*, "Origins and Evolution of Antibiotic Resistance". Microbiol Mol. Biol. Rev. *74*, 2010,433. https://doi.org/10.1128/mmbr.00016-10

[3]. *H. Schiff*, Mittheilungen aus dem Universitätslaboratorium in Pisa: Eine neue Reihe organischer Basen. Jus. Liebigs Ann. der. Chem. 131, 1864,119.

[4]. *S. Arulmurugan, H.P. Kavitha, and B.R. Venkatraman*, Biological activities of Schiff base and its complexes: A review. Rasayan J. Chem. 3, 2010, 410.

[5]. *A.A. Jarrahpour, M. Motamedifar, K. Pakshir, N. Hadi, and M. Zarei*, Synthesis of novel azo Schiff bases and their antibacterial and antifungal activities. Mol. 9, 2004, 824. https://doi.org/10.3390/91000815

[6]. *S.N. Pandeya, S. Smitha, M. Jyoti, and SK.* Sridhar, Biological activities of isatin and its derivatives. Acta. Pharm. 55, 2005, 46.

[7]. *J. Iqbal, S.A. Tirmizi, F.H. Wattoo, M. Imran, M.H.S. Wattoo, S. Sharfuddin and S. Latif* , Biological Properties of Chloro-salicylidene Aniline and Its Complexes with Co(II) and Cu(II). Turk. J. Biol. 30, 2006, 4.

[8]. *N. Aggarwal, R. Kumar, P. Dureja, D.S. Rawat*, Schiff base as potential fungicides and nitrification inhibitors. J. Agric. Food Chem. 57, 2009, 8525. https://doi.org/10.1021/jf902035w

[9]. *A.O. De Souza, F.C.S. Galetti, C.L. Silva, B. Bicalho, M. Parma, S.F. Fonseca, A.J. Marsaioli, A.C.L.B., Trindade, Freitas, RP. Gil, F.S. Bezerra*, Antimycobacterial and cytotoxicity activity of synthetic and natural compounds. Quim Nova, 30, 2007, 1566. https://doi.org/10.1590/S0100-40422007000700012

[10]. *F. Cheng, W. Li, Y. Zhou, J. Shen, Z. Wu, G. Liu, P.W. Lee, Y. Tang*, admetSAR: a comprehensive source and free tool for assessment of chemical ADMET properties. J. Chem. Inf. Model. 52, 2012, 3105. https://doi.org/10.1021/ci300367a.

[11]. *W. Zeyuan, M. Erickson*, Paragas, Swati Nagar and Ken Korzekwa, Complex Cytochrome P450 Kinetics Due to Multisubstrate Binding and Sequential Metabolism. Part 1. Theoretical Considerations. Drug. Metab. Dispos. 49, 2021, 1099. https://doi.org/10.1124/dmd.121.000553.

[12]. *M.P. Gleeson, A. Hersey, S. Hannongbua,* In-silico ADME models: a general assessment of their utility in drug discovery applications. Curr. Top. Med. Chem. 11, 2011, 381. https://doi.org/10.2174/156802611794480927.

[13]. V. Gupta, S. Singh, Y.K. Gupta, (). Synthesis and Antimicrobial Activity of some Salicylaldehyde Schiff bases of 2-aminopyridine. Res. J. Chem. Sci. 3, 2013, 29.

[14]. T. Sevenet, C. Tortora, Plants molecules and drugs Nathan. CNRS, Editions Paris, 1994.

[15]. *A. D. Becke*, Density-functional thermochemistry. III. The role of exact exchange, *J. Chem. Phys*., 98, 1993, 5648-5652. https://doi.org/10.1063/1.464913.

[16]. *C. Lee, W. Yang, G. R. B. Parr*, (1), Development of the Colic-Salvetti correlation-energy formula into a functional of the electron density. *Phys. Rev*. 37, 988, 785-789. https://doi.org/10.1103/PhysRevB.37.785.

[17]. *M.J. Frisch, G.W. Trucks, H.B. Schlegel, G. E. Scuseria, M.A. Robb, J.R. Cheeseman*, Gaussian 09, Revision A. 02, Gaussian Inc Wallingford CT., 34, Wallingford CT, 2009.

[18]. *I. Grib, M. Berredjem, K.Otmane Rachedi, S. E. Djouad, S.Bouacida, R. Bahadi, Tan-Sothea Ouk, M. Kadri, T. Ben Hadda, B. Belhani*, Novel N-sulfonylphthalimides: Efficient synthesis, X-ray characterization, spectral investigations, POM analyses, DFT computations and antibacterial activity, J. Mol. Struct, 1217, 2020, 128423.

[19]. *D. Liotta, Advances in Molecular Modeling*,1, Ed. JAI Press, 1988.

[20]. *J.S. Murry, K. Sen*, , Theoretical and computational chemistry (3) - Molecular electrostatic potential, concepts and applications. Vol:1 Mol. *Elesvier*, 1996, 664. ISBN: 0 444 82353 0.

[21]. *I. Alkorta, J.J. Penez*, Molecular Structure, Dynamics, and Function of Biological Systems - Molecular polarization potential maps of the nucleic acid bases. *Int. J. Quantum Chem*. 57, 1996, 123-135. https://doi.org/10.1002/(SICI)1097-461X(1996)57:13.0.CO;2-9.

[22]. *F.J. Luque, M. Orozco, P.K. Bhandane, S.R. Gadge*, "SCRF calculation of the effect of water on the topology of the molecular electrostatic potential". *J. Phys. Chem*. 97, 1993, 9380-9384. https://doi.org/10.1021/j100139a021.

[23]. *H., Pham The, I. González-Álvarez, M. Bermejo, V. Mangas Sanjuan, I. Centelles, T.M. Garrigues, and M.Á. Cabrera-Pérez*, In Silico Prediction of Caco-2 Cell Permeability by a Classification QSAR Approach. Mol. Inf. 30, 2011, 385. https://doi.org/10.1002/minf.201000118.

[24]. *S.Ruswanto, M. Richa, N. Tita, L. Tresna*, Molecular Docking of 1- Benzoyl-3-Methylthiourea as Anti Cancer Candidate and Its Absorption, Distribution, and Toxicity Prediction. J. Pharm. Sci. & Res. 9, 2017, 684.

[25]. *V.M. Alves, E. Muratov, D. Fourches, J. Strickland, N. Kleinstreuer, C. H. Andrade, A. Tropsha*, Predicting chemically-induced skin reactions. Part II: QSAR models of skin permeability and the relationships between skin permeability and skin sensitization. Toxicol. Appl. Pharmacol. 284, 2015, 280. https://doi.org/10.1016/j.taap.2014.12.013.

[26]. *C. Suenderhauf, F. Hammann, J. Huwyler*, Computational prediction of blood-brain barrier permeability using decision tree induction. Molecules. 17, 2012, 10445. https://doi.org/110.3390/molecules170910429.

[27]. *G. Berellini, C. Springer, N.J. Waters, F. Lombardo, In silico* prediction of volume of distribution in human using linear and nonlinear models on a 669 compound data set. J. Med. Chem. 52, 2009, 4495. https://doi.org/10.1021/jm9004658.

[28]. *J.W.T. Yates, P.A. Arundel*, On the volume of distribution at steady state and its relationship with two-compartmental models. J. Pharm. Sci. 97, 2008, 122. https://doi.org/10.1002/jps.21089.

[29]. *U.M. Zanger and M. Schwab*, Cytochrome P450 enzymes in drug metabolism: regulation of gene expression, enzyme activities, and impact of genetic variation. Pharmacol Ther. 138, 2013, 141. https://doi.org/10.1016/j.pharmthera.2012.12.007.

[30]. *A. Schmidt, A. Braeuning P. Ruck, G. Seitz, S. Armeanu-Ebinger, J. Fuchs, S.W. Warmann, M. Schwarz*, Differential expression of glutamine synthetase and cytochrome P450 isoforms in human hepatoblastoma. Toxicology. 281, 2011, 14. https://doi.org/10.1016/j.tox.2011.01.006.

[31]. *Y. Wang, J. Xing, Y. Xu, N. Zhou, J. Peng, Z. Xiong, X. Liu, X. Luo, C. Luo, K. Chen, M. Zheng*, In silico ADME/T modelling for rational drug design. *Quarterly Reviews of Biophysics,48*, 4, 2015, 488-515. https://doi.org/10.1017/S0033583515000190.

[32]. *S.J. Caldwell, Y. Huang, A.M. Berghuis*, Antibiotic Binding Drives Catalytic Activation of Aminoglycoside Kinase APH(2″)-Ia. Structure, 24, 2016, 45. https://doi.org/10.1016/j.str.2016.04.002

[33]. *D.E. Rollins, C.D. Klaassen*, Biliary excretion of drugs in man. Clinical Pharmacokinetics. 4, 1979, 379. https://doi.org/10.2165/00003088-197904050-00003

[34]. *S.L. Samodelov, G.A. Kullak-Ublick, Z. Gai, M. Visentin*, Organic Cation Transporters in Human Physiology, Pharmacology, and Toxicology. Int. J. Mol. Sci. 21, 2020, 7890. https://doi.org/10.3390/ijms21217890.

[35]. *H. Koepsell*, Multiple binding sites in organic cation transporters require sophisticated procedures to identify interactions of novel drugs. Biol. Chem. 400, 2019, 207. https://doi.org/10.1515/hsz-2018-0191.

[36]. *C.A. Lipinski, F. Lombardo, B.W. Dominy, P. J. Feeney*, Experimental and computational approaches to estimate solubility and permeability in drug discovery and development settings. Adv. Drug Deliv. Rev. 23, 1997, 25. https://doi.org/10. 1016/S0169-409X(96)00423-1.

[37]. *D.F. Veber, S.R. Johnson, H.Y. Cheng, B. R. Smith, K.W. Ward, & K.D. Kopple*, Molecular properties that influence the oral bioavailability of drug candidates. J. Med. Chem. 45, 2002, 2623. https://doi.org/110.1021/jm020017n.

[38]. *O.A. Raevsky, V.Y. Grigorev, D.E. Polianczyk, G.I. Sandakov, S.L. Solodova, A.V. Yarkov, S.O. Bachurin, J.C. Dearden*, Physicochemical property profile for brain permeability: comparative study by different approaches. J. Drug. Target. 24, 2016, 662. https://doi.org/ 10.3109/1061186X.2015.1132224.

[39]. *N. J. Yang, M.J. Hinner*, Getting across the cell membrane: an overview for small molecules, peptides, and proteins. *Methods mol. biol. 1266*, 2015, 53. https://doi.org/10.1007/978-1-4939-2272-7_3.

[40]. *H. Van de Waterbeemd, G. Camenisch, G. Folkers, J.R. Chretien, O.A. Raevsky*, Estimation of blood-brain barrier crossing of drugs using molecular size and shape, and H-bonding descriptors. J. Drug. Target. 6, 1998, 165. https://doi.org/1doi: 10.3109/10611869808997889.

[41]. *J.A. Platts, M.H. Abraham, Y.H. Zhao, A. Hersey, L. Ijaz, D. Butina*, Correlation and prediction of a large blood-brain distribution data set--an LFER study. Eur. J. Med. Chem. 36, 2001, 730. https://doi.org/10.1016/s0223-5234(01)01269-7.

[42]. *H. Van De Waterbeemd, G. Camenisch, G. Folkers, O.A. Raevsky*, Estimation of Caco-2 Cell Permeability using Calculated Molecular Descriptors. Quant. Struct-Act Relatsh, 15, 1996, 490. https://doi.org/10.1002/qsar.19960150604.

[43]. *U. Norinder, M. Haeberlein*, Computational approaches to the prediction of the blood-brain distribution. Adv. Drug. Deliv. Rev. 54, 2002,313. https://doi.org/110.1016/s0169-409x(02)00005-4.

[44]. *M. Iyer, R. Mishra, Y. Han, A.J. Hopfinger*, Predicting blood-brain barrier partitioning of organic molecules using membrane-interaction QSAR analysis. Pharm. Res. 19, 2002, 1621. https://doi.org/10.1023/a:1020792909928.

[45]. *T.I. Oprea*, Property distribution of drug-related chemical databases. J. Comput. Aided Mol. Des. 14, 2000, 264. https://doi.org/10.1023/a:1008130001697.

[46]. *F. Ooms, P. Weber, P.A. Carrupt, B.A. Testa*, Simple model to predict blood-brain barrier permeation from 3D molecular fields. Biochim. Biophys. Acta. 1587, 2002, 125. https://doi.org/10.1016/S0925-4439(02)00074-1.

[47]. *A.K. Ghose, V.N. Viswanadhan, J.J. Wendoloski*, A knowledge-based approach in designing combinatorial or medicinal chemistry libraries for drug discovery. 1. A qualitative and quantitative characterization of known drug databases. J. Comb. Chem. 1, 1999, 68. https://doi.org/10.1021/cc9800071.

[48]. *C.R. Ellis, R. Racz, N.L. Kruhlak, M.T. Kim, E.G. Hawkins, D.G. Strauss, L. Stavitskaya*, Assessing the Structural and Pharmacological Similarity of Newly Identified Drugs of Abuse to Controlled Substances Using Public Health Assessment via Structural Evaluation. Clin. Pharmacol. Ther. 106, 2019, 122. https://doi.org/10.1002/cpt.1418.

[49]. *A. Daina, V. Zoete*, A BOILED-Egg To Predict Gastrointestinal Absorption and Brain Penetration of Small Molecules. Chem. Med. Chem. 11, 2016, 1121. https://doi.org/10.1002/cmdc.201600182.

[50]. *J. Kelder, P.D. Grootenhuis, D.M. Bayada, L.P. Delbressine, J.P. Ploemen*, Polar molecular surface as a dominating determinant for oral absorption and brain penetration of drugs. Pharm. Res. 16, 1999, 1519. https://doi.org/10.1023/a:1015040217741

[51]. *Y.C. Zheng, B. Yu, G.Z. Jiang, X.J. Feng, P.X. He, X.Y. Chu, W. Zhao, H.M. Liu*, Irreversible lsd1 inhibitors : application of tranylcypromine and its derivatives in cancer treatment. Curr. Top. Med. Chem. 16, 2016, 2188. https://doi.org/10.2174/1568026616666160216154042

[52]. *M.Y. Belghit, A. Moussi, and D. Barkat*, *In vitro* antifungal activity of some Schiff bases derived from *ortho*-hydroxybenzaldehyde against fusarium. J. Eng. Sci. Technol, 12, 2017, 1722.

[53]. *C.M. Mann, and J.L, Markham* A new method for determining the minimum inhibitory concentration of essential oils. J. Appl. Microbiol. 84, 1998, 544. https://doi.org/10.1046/j.1365-2672.1998.00379.x

[54]. *J. Caldwell, I. Gardner, N. Swales*. An Introduction to Drug Disposition: The Basic Principles of Absorption, Distribution, Metabolism, and Excretion. Toxicol. Pathol. 23, 1995, 114. https://doi.org/10.1177/019262339502300202.

[55]. *D.E.V. Pires, T.L. Blundell, D.B. Ascher*, pkCSM: Predicting Small-Molecule, 2015.

[56]. *A. Daina, O. Michielin, and V. Zoete*, SwissADME*:* A free web tool to evaluate pharmacokinetics, drug-likeness and medicinal chemistry friendliness of small molecules. Scientific Reports. 7, 2017, 421717. https://doi.org/doi: 10.1038/srep42717.